Italian Journal of Geosciences
Bollettino della
Società Geologica Italiana
e del Servizio Geologico d'Italia

ISPRA
Istituto Superiore per la Protezione e la Ricerca Ambientale
Dipartimento per il
SERVIZIO GEOLOGICO D'ITALIA
Organo Cartografico dello Stato (legge N°68 del 2.2.1960)

Earthquake weak motions and noise measurements unravel significant site amplification effects in the Val d'Agri complex basin (southern Italy)

Journal:	*Italian Journal of Geosciences*
Manuscript ID	IJG-2021-0965
Manuscript Type:	Original Article
Date Submitted by the Author:	13-Jun-2021
Complete List of Authors:	pucillo, stefania; INGV, Roma 1 Riccio, Gaetano; INGV, Roma 1 Fodarella, Antonio; INGV, Roma 1 Cogliano, Rocco; INGV, Roma 1 Improta, Luigi; INGV, ONT
Keywords:	site effects, Val d'Agri, spectral ratios, 2D modeling

Earthquake weak motions and noise measurements unravel significant site amplification effects in the Val d'Agri complex basin (southern Italy)

S. Pucillo [(1)], G. Riccio [(1)], A. Fodarella [(1)], R. Cogliano [(1)], L. Improta [(2)]

(1) Istituto Nazionale di Geofisica e Vulcanologia, Sismologia e Tettonofisica, Contrada Ciavolone, Grottaminarda (Italy)

(2) Istituto Nazionale di Geofisica e Vulcanologia, Osservatorio Nazionale Terremoti, Via di Vigna Murata 605, Roma (Italy)

Corresponding author S. Pucillo, stefania.pucillo@ingv.it

Abstract

The Val d'Agri basin is one of the areas of highest seismic hazard in Italy. Moreover, widespread residential buildings with high seismic vulnerability, a medium size water reservoir, and infrastructures related to hydrocarbon exploitation contribute to increasing the local seismic risk. The basin is several kilometers wide and filled by more than 500 m of fan, alluvial and lacustrine deposits dating back to the Middle Pleistocene – Holocene. Ground motion amplifications are expected due to such a local geological setting. In this paper we analyze for the first time earthquake weak ground motions and ambient noise measurements to investigate local site effects.

Data presented here were recorded by eight seismic stations deployed along a 7 km long transect that runs SW-NE across the central part of the basin. The stations operated for about three years; four of them were installed within the basin, two near its edges, and two outside on limestone outcrops.

Good quality recordings from more than forty local and regional earthquakes (with ML in the 1.4 - 5.5 range) evidence significant ground motion amplification both in the peak values and durations for the basin stations relative to the hard-rock one. Site effects have been investigated by computing: (1) standard spectral ratios with respect to the hard-rock station (H/Hrif), (2) single-station H/V spectral ratios, (3) simplified 1-D and 2-D numerical modelling based on accurate subsurface information.

Earthquake recordings for sites within the basin show: (i) significant ground motion amplifications in a wide frequency range (0.5-7 Hz), (ii) a dominant low-frequency peak around 0.7 - 1 Hz with amplification factors between 3 and 7, (iii) secondary peaks around 1.5

Hz and 3 Hz. Single-station techniques provide consistent results. H/V ratios show a clear peak or bump around 0.6 - 1 Hz that matches that obtained by the site-reference analysis and allows us to pinpoint the fundamental resonance frequency of the sites. The evidence for a low-frequency peak provided by both the H/Hrif and H/V spectral ratios is consistent with the available subsurface information on the basin architecture.

Frequency-time and particle motion analysis performed on earthquake data indicate that both S-waves (t=5-10 s) and later arrivals contribute to amplify ground motion below 1 Hz. Significant low-frequency amplifications can occur up to 35 s after direct S-waves and are mainly due to arrivals of horizontal polarized waves propagating in the basin (Love phases). Taken together, these observations indicate that the observed ground motion amplifications cannot be entirely explained by simple 1D propagation effects, so we carried out several 2-D numerical simulations of the basin in order to better investigate the local seismic response. The results evidence a role played by basin edge effects on the observed ground motion amplifications. In addition, the basin response is controlled by strong internal heterogeneities between high-velocity stiff sediments filling the eastern depocenter of the basin and low-velocity softer deposits widespread in the central-western sector of the basin.

Keywords: site effects, Val d'Agri, spectral ratios, 2D modeling

1. Introduction

The Val d'Agri (hereinafter VAB) is one of the largest continental tectonic basins of the Apennines seismic belt of Italy (Figure 1). The basin, elongated for 25 km in the NW-SE direction and up to 7-km-wide, is located in the Lucania arc of the southern Apennines, one of

the regions with highest seismic hazard in Italy. It was struck in 1857 by a M7 earthquake that caused more than 30,000 casualties and raised to the ground all the local villages (Mallet 1862; Burrato and Valensise, 2008). Since 1857 the VAB experienced only M4+ moderate events (Stabile et alii, 2015). Instrumental seismicity recorded in the last 20 yrs after the deployment of numerous local permanent stations of the RSN and ENI monitoring networks is characterized by weak sparse events and small swarms seldom exceeding M3. A part of this activity is ascribed to two well documented cases of anthropogenic microseismicity induced by a water reservoir (Valoroso et alii, 2009; Stabile et alii, 2014) and by fluid injection into a disposal well (Improta et alii, 2015; Improta et alii, 2017).

The causative fault of the 1857 is uncertain and it is ascribed either to the NE-dipping MMFS normal fault system bounding the basin to the west or to the SW-dipping EAFS trastensive fault system bounding the basin to the east (Maschio et alii, 2005; Cello et alii, 2003) (Fig. 1). Both fault systems are structured into km-long sub-parallel active fault splays, reach a total length of 30-40 km and are considered potential source of M6-7 normal faulting events (Cello et alii, 2003; Maschio et alii, 2005; Improta et alii, 2010).

The Quaternary basin is mainly filled by Middle Pleistocene - Holocene continental sediments up to 500 m thick that overlay and articulated Mesozoic-Tertiary substratum (Dell'Aversana, 2003) (Figure 1). High-resolution seismic tomography surveys based on a commercial profile acquired with a non conventional dense-wide-aperture geometry (Morandi e Ceragioli, 2002; Improta et alii, 2008) show that the low-velocity continental infill is delimited on the both sides of the basin and at its bottom by strong and sharp velocity variations (the trace of the seismic profile is shown in Fig. 1). Typically, km-scale deep sedimentary basins associated to strong vertical and lateral heterogeneities, as those of the VAB, are the locus of significant ground motion amplification effects in a wide frequency range (0.2 - 10 Hz), that can increase the peak

values and durations of shaking during moderate-strong earthquakes, thereby contributing to increase seismic hazard (Graves and Wald, 2004; among others). Furthermore, the local villages are characterized by a high percentage (40%) of residential buildings with very-high seismic vulnerability (Masi et alii, 2021), while the area hosts industrial infrastructure mainly related to hydrocarbon exploitation (Borfecchia et alii, 2016) and a medium size water reservoir (i. e. Pertusillo Lake, Figure 1).

It arises from previous considerations that the knowledge of the basin response is of key importance for a reliable seismic hazard assessment. Nevertheless, the VAB has never been the target of a specific local site effects study aimed at investigating the basin response by earthquake recordings. This manuscript represents the first attempt to bridge this information gap. We present the result of the analysis of weak motion recordings of local and regional earthquakes and ambient noise collected at eight temporary seismic stations operated by INGV between 2006 and early 2009. These stations were deployed in the central, deeper sector of the basin, along the seismic profile of Morandi and Ceragioli (2002) in order to take advantage of valuable constraints on the subsurface structure. Two stations were installed near both basin edges on the western ridge above Mesozoic limestones (AG13) and on the eastern slope above stiff cemented breccias covering the nearly outcropping limestones (AG44). The remaining six stations were deployed inside the basin on recent alluvia and fan deposits. Seismic recordings were analyzed by classical spectral techniques (Borcherdt 1970, Field et alii, 1995) to determine the dominant frequency response of the sites and the relative ground motion amplifications with respect to the bedrock reference site AG13. The six basin sites show significant differences in the seismic response that was first investigated by simple 1D numerical modelling. To improve understanding of the basin seismic response we complemented the study with 2D numerical simulations based on a finite difference technique

and on a model setup constrained by subsurface exploration data and then redefined by comparing the results of numerical modelling with those from on-site recordings.

2. Geologic setting and basin structure

The Val d'Agri is a Quaternary continental basin whose genesis and evolution has been controlled by the two NW-SE trending and oppositely dipping range-bounding normal-fault systems: the west-dipping Eastern Agri Fault system to east and the east-dipping Monti della Maddalena fault system to the west (Figure 1; Cello et alii, 2003; Maschio et alii, 2005). The basin is filled by slope breccias, alluvial fan deposits and fluvio-lacustrine sequences dating back to Middle Pleistocene and Holocene (Zembo et alii, 2009) that unconformably overlay an articulated substratum consisting of Meso Cenozoic carbonate platform, deep basin and flysch sequences (Figure 1). The infill reaches a maximum thickness in the central part of the basin. Here, a deep oil well penetrated Quaternary continental deposits 440 m thick above Mesozoic platform limestone (Dell'Aversana, 2003). Our seismic experiment focused on this sector of the basin (Figure 2) for the following reasons: (1) the presence of the deeper basin depocenter, (2) the existence of a strong velocity contrasts and the basin bottom and edges due to high-velocity Mesozoic limestones underlying the Quaternary sediments, (3) an high-resolution crustal seismic profile provides key constraints on the basin geometry, internal architecture and velocity structure. This seismic profile crosses with a SW-NE strike the basin and both bounding ridges and was acquired with a non-conventional wide-aperture multifold acquisition geometry (Dell'Aversana et alii, 2003). P-wave tomography surveys (Morandi and Ceragioli, 2002; Improta et alii, 2008) evidence an asymmetric shape of the basin due to the presence of a major basin depocenter under its eastern side (Figure 3).

In addition, the basin interior can be subdivided into two main zones based on the nature of the sedimentary infill. The eastern sector is characterized by a wedge-shaped complex of coarse

clastic sediments mainly consisting of Middle Pleistocene - Upper Pleistocene cemented slope breccias and alluvial fan conglomerates (Figures 2 and 3). These deposits attain relatively high P-wave velocities (2000-2500 m/s) and overlay a fault dissected substratum consisting of Mesozoic limestones with velocities in the range 4000-4800 m/s (Figure 3). In the central-western sector the infill consists of Upper Pleistocene alluvial and fluvio-lacustrine sequences. These deposits attain lower V_P in the range 1000-2000 m/s and lay on the limestone substratum. The shallowest sediments consist of loose to dense Late Pleistocene - Holocene sediments (recent alluvia and fan deposits) with P-wave velocities lower than 1000 m/s. These recent sediments form a shallow cover that tends to thicken south-westward.

Based on the described subsurface velocity structure low frequency site effects are expected, as inferred by preliminary analysis of ambient seismic noise data (Mucciarelli et alii, 2005).

3. The seismic experiment

Starting from January 2006 we installed four seismic stations (AAP, AAS, CFS, ITS in Figures 2 and 3) along a SW-NE profile, transversal with respect to the central part of the basin and nearly collocated with the seismic seismic line of Dell'Aversana (2003). Subsequently (January 2007) we deployed two more stations, BNF and LMB, closer to the edges of the basin to better investigate border effects. These stations are located on recent alluvia with the exception of BNF that was deployed on coarse fan deposits (Figure 2). Two seismic stations located outside the basin on the western and eastern limestone ridges (AG13 and AG44, respectively) also contributed to the experiment as reference sites.

The seismic experiment halted in March 2009. Each station consisted of a Quanterra Q330 (https://www.q330.com) or a Reftek 130 digitizer (https://www.reftek.com), equipped with three-component velocimeters (all of the model Le3D-5s manufactured by Lennartz, https://www.lennartz-electronic.de) and accelerometers Episensor by Kinemetrics

(https://www.kinemetrics.com) or 131A02/3 by RefTek (now discontinued). Both sensors were partially buried in order to improve the seismic coupling with the ground. Each station was equipped with a GPS antenna for synchronization. Velocimeters used in the experiment show flat amplitude response between 0.2 and 50 Hz, and are characterized by very low electronic noise (rms < 1 nm/s at 1 Hz); full scale range of accelerometers was set to at least 1 g. All stations operated in continuous modality.

During the experiment the network recorded 81 earthquakes, characterized by a good signal-to-noise ratio in the frequency band of interest (0.2 - 10 Hz). The events were mostly regional with magnitude up to 5.7 and localized in the Balkan peninsula, near the Calabrian coasts, in the Gargano area or in the southern Tyrrhenian Sea, therefore with a back azimuth between 0° and 180°; the few local events used for the survey were small magnitude events (M < 3) located to the north of the VAB in the Campanian sector of the southern Apennines (Figure 4).

4. Results from analysis using classical spectral techniques, time-frequency analysis and 1-D numerical methods

Standard Spectral Ratios (SSR) method is widely used for site effects studies; it consists in evaluating spectral ratios between homologous components of seismic motion at a generic station and at a reference site, that is assumed to be not affected by local amplification phenomena. Its purpose is to get an estimate of the transfer function of the site under investigation (Borcherdt, 1970).

Horizontal to Vertical Spectral Ratios (HVSR) consists in calculating the ratio between horizontal and vertical components of the ground motion at a site. If applied to ambient seismic noise, it is also known as Nakamura method (Nakamura, 1989); in this case it is very fast and inexpensive to apply because it doesn't require the use of earthquakes, but it is not reliable for estimating the ground motion amplification factors (e. g. Lachet et alii, 1994), whereas it

provides very satisfactory results for the estimation of resonance frequencies when the local velocity structure is relatively simple and characterized by low-velocity sediments above an high velocity bedrock. In Sesame 2005 very comprehensive (and widely used in geophysics) guidelines are reported on the method of data processing and preprocessing, and on interpretation of results.

In this study we computed SSR for earthquake recordings and HVSR for earthquake and ambient seismic noise to investigate the seismic response of the basin.

The SSR technique requires the choice of a reference station. In order to select the reference between the two stations installed on bedrock, we used the HVSR technique applied both to ambient seismic noise and earthquakes. Both sites turned out to be good as a reference because the mean H/V curves were substantially flat (Figure 5). We preferred to use the AG13 station because it showed a better signal-to-noise ratio on the earthquakes taken into consideration.

An example of recordings of regional event is shown in Figure 6. The figure reports the waveforms of the horizontal components of motion for the Mw 3.8 earthquake located at a distance of150 km from the VAB (origin time 2007-03-26 13:55:26) recorded by all six stations in the basin and by the reference AG13. We note that the signal to noise ratio is good for all the sites, and the seismograms are clearly distinguishable from the background ambient noise, observable in the first few seconds of the plot, before the arrival of the P waves. All stations in the basin show ground motion amplification with respect to the reference site AG13. Also, ground motion duration increases for stations in the central part of the basin (see for example AAS). The seismic response is very variable from one station to another. In particular, stations located at the basin edges (BNF and LMB) show a lower ground motion amplification with respect to those installed inside (from AAP to ITS) and between them BNF the one that presents the most reduced amplification.

SSR analysis on earthquakes was carried out by calculating, for each earthquake, the spectral ratio between the homologous components of the seismic motion at each of the stations in the basin and at the reference site, and then making the geometric mean of all the single H/H curves. The average curves with associated standard deviations are shown in Figure 7 for all the stations.

If we consider an amplification threshold of two, we observe for all the stations amplifications for the horizontal components with respect to the reference AG13 in a wide range of frequencies (i. e. from 0.5 - 0.8 Hz up to about 5 Hz, depending on the station). We observe average amplification factors as large as 7 (station ITS). The vertical component of the motion (not shown in the figure) is not affected by significant amplifications, for any of the stations in the basin. Interestingly, moving along the transect from north-east to south-west while excluding site BNF, the amplifications on the horizontal components show increasing factors from 4 to 6 and affect a wider range of frequencies, with the upper limit moving from 2 Hz to 5 Hz.

Analyzing the stations individually starting from the north-east edge of the basin, we can see that station BNF shows the main amplification peak between 0.8 and 0.9 Hz, with an amplification factor of about 2. This peak value is significantly lower with respect to that computed at the four stations in the center of the basin. This observation is compatible with the fact that the local soil conditions of BNF are characterized by a thick sequence of coarse cemented deposits (fan conglomerates and breccias) above the limestone substratum (Figure 3). Station AAP has a fundamental frequency between 0.6 and 0.7 Hz, with a corresponding amplification factor of up to 4 for the N-S component; the frequency range affected by significative amplification (> 2) with respect to AG13 is 0.5 - 2 Hz. Stations AAS and CFS show a fairly similar behavior, with the main amplification peak at about 0.7 Hz and the

amplification factor of 5. The frequency range of significant relative amplification extends from 0.5 to 3 Hz.

Station ITS shows the strongest amplifications. The main peak indicative of the fundamental frequency of the site is found between 0.7 and 0.8 Hz and the peak amplitude exceeds the value of 6. The frequency range with an amplification of the motion above 2 is about 0.5 - 5 Hz.

The site LMB at the south-west basin edge exhibits the maximum amplification relative to AG13 (around 3-4) between 1 and 2 Hz, therefore at frequency higher with respect to previous stations. This is in agreement with the shallower basin substratum along its western edge (Figure 3). For this station the frequency range affected by amplification is about 0.8 - 5 Hz.

For all stations but ITS the behavior in the high frequency range is quite regular. The relative amplification gradually decreases and no clear secondary peaks are observed. Station ITS (component N-S) instead shows significant secondary peaks between 1 and 2 Hz and between 3 and 4 Hz.

As to the single-station technique (HVSR), we chose to perform the ambient noise analysis on two hour recordings, and we referred to the guidelines outlined in Sesame 2005 for processing. For the analysis on earthquakes we selected the events following the same criterion used for the SSRs. The resulting H/V curves are shown in Figure 8a-b. We observe that all stations show a clear low-frequency peak or bump. The fundamental frequency of the site inferred from such peaks of the H/V curves is in overall good agreement with that estimated by the SSR technique.

For the four stations in the central part of the basin, we found that the fundamental resonance frequency estimated by SSR analysis can be reproduced by transfer functions for S waves with a 1-D numerical model using the Thomson-Haskell technique (Haskell, 1960). We used the high-resolution P-velocity tomogram of Improta et alii (2008) to set up the 1-D modelling

(Figure 3, upper panel). As basin limestone substratum we assumed the 4.5 km/s iso-velocity line in agreement with subsurface geologic constraints (Dell'Aversana, 2003) (Figure 3, lower panel). The parameters assumed for the bedrock were V_P 5.5 km/s, V_P/V_S = 1.8, density ρ = 2.6 t/mc. For the basin sites, we derived the V_S from average V_P tomographic values and setting the V_P/V_S ratio to 2.2. The thickness of the sediment layer is constrained by the tomographic model and the density is set to ρ = 2.0 t/mc. Density values are based on results of gravity data modelling (Dell'Aversana, 2003). The resulting S-wave velocities and thicknesses for the surface layer in the 1-D models of the various stations are reported in Table 1. The theoretical transfer function for station AAS is shown in Figure 9. The theoretical fundamental resonant frequency obtained from the 1-D modelling is consistent with that estimated using spectral methods on earthquakes and ambient noise. However, the 1-D modeling underestimates the amplitude of the low-frequency fundamental peak, as well as the amplification factor at higher frequencies. The same results were obtained at the remaining three sites. Besides, this approach of 1-D modelling was not able to reproduce the fundamental resonance frequency at the two edge sites BNF and LMB.

We also analyzed in detail a moderate local event (ML 3.9) of the Lucanian-Campanian Apennines; the event occurred at a depth of 27 km, distance from the station 41 km, and back azimuth 47 °N. The waveforms for all stations including the reference site, previously filtered between 0.1 and 2.0 Hz, are shown in Figure 10. The longer duration of the earthquake compared to the reference site AG13 is evident for the stations in the basin and it is due to late arrivals (compared to direct S waves), very energetic at low frequencies. The amplifications of the seismic motion for this event are very high, with the maximum amplification factor ranging between 5 on site AAP and 10 on ITS (Figure 11).

We carried out time - frequency analysis on this event for sites AG13 and AAS, and the result is shown in Figure 12. We note that both the S waves (t = 5-10 s) and the secondary arrivals, consisting of surface waves, contribute to amplify the seismic motion below 1 Hz. Site AAS exhibits significant low frequency amplifications even up to 35 s after direct S waves, time corresponding to 650 s in the plot.

The particle motion in Figure 13 (right panel) was performed on a portion of the signal containing the very energetic arrival observed on site AAS. The time window used, beginning at the time t1 = 639.5 s and ending at t2 = 641.5 s, is the portion delimited by the two vertical lines in Figure 13 (left panel). The particle motion plot suggests the presence of horizontally polarized surface waves (Love waves) that are generated in the basin, possibly at the basin edges.

Summarizing the information derived from the various analyzes carried out, the results obtained with the classic SSR technique show a significant amplification in a wide range of frequencies and a low-frequency dominant peak (0.7-1 Hz, depending on stations), with corresponding amplification factors between 2 and 6. The trend of the seismic response is quite different between one station and another both in terms of fundamental frequencies and of amplification factors and range of frequencies involved. From the trend of curves in the high frequency range, we deduce that there are strong amplification effects far beyond the fundamental frequencies, even if we do not observe clear secondary peaks.

Single-station H/V ratios also show the dominant low-frequency peak, but the amplification factors are clearly underestimated. Similarly, 1-D modelling can reproduce the position of the fundamental resonance peak for sites in the center of the basin, but it underestimates the amplification factors.

Furthermore, frequency-time and particle motion analysis shows that the surface waves contribute to the low frequency amplification even up to several seconds after the direct S waves, and they are mainly due to the Love waves propagating in the basin. All these considerations led us to conclude that the observed site effects amplifications could not be fully explained by simple 1-D propagation effects but they can be ascribed to a 2D or even 3D behavior of the basin structure.

4. 2-D numerical modeling

To carry out the 2D numerical simulations we used a calculation program made available by CASPUR consortium (Consorzio interuniversitario per le Applicazioni di Supercalcolo Per l'Università di Roma) and by INGV researchers through W.I.S.A. (Web Interface for Seismological Applications, Santoni et alii, 2004). Unfortunately the program and the W.I.S.A. interface are no longer maintained and now are discontinued. The program receives in input the structure of the (two-dimensional) domain under investigation, the physical parameters (velocity, density, quality factor) of the various areas into which it is divided, the distance of the source from the free surface, the total simulation time, the type of source (i. e. point-like source for PV simulation or plane wave for SH one; in the latter case you can choose the angle of incidence). The source is a Gabor impulse, of the form:

$$G(t) = \exp(-[2\pi f_p(t-t_s)/\gamma]2)\ \cos[2\pi f_p(t-t_s)+\phi]$$

In this expression f_p is the dominant frequency, and together with γ determines the pulse width; this type of forcing term is very convenient because its parameters can be modified to ensure that the spectrum covers the entire frequency range of interest. The domain of investigation is discretized in a regular (two-dimensional) grid; the spatial step of the grid and the sampling period are automatically determined on the basis of the geological and physical characteristics of the various areas and the maximum frequency of interest. The program applies in the SH

case a finite-differences approach (Caserta, 1998) whereas it uses a finite-elements approach for the case of P-SV waves (Lanucara et alii, 2004). It simulates the propagation of seismic waves within the domain and the reflections and refractions at the interfaces between the various zones (Caserta et alii, 2002); in output the synthetic seismograms on the free surface are obtained; they have dimensions of a displacement, and are equally spaced from each other.

For our simulations we chose a plane wave source (SH case), with vertical incidence and parameters used for the Gabor function $f_p = 0.45$ and $\gamma = 0.066$; we constrained the basin structure using the tomographic survey of Improta et alii (2008). We made the association between sites of simulations and real seismic stations by projecting these latter on the 2-D model given in input to the code (i. e., the velocity section) according to the general trend of the Quaternary basin bounding faults. This association can have an uncertainty in the order of a few hundreds of meters due to possible 3-D heterogeneities in the basin structure and due to the unknown real geometry of the buried substratum faults. For each simulation we calculated the spectral ratios between the waveform provided in output for each site corresponding to a real seismic station and the synthetic waveform obtained at the depth of the source (once deprived of the part due to reflection on the free surface, to ensure that it represented only the incident wave). We then compared the computed spectral ratios (hereinafter simulated spectral ratios) with those obtained for each seismic statins by applying the SSR technique to earthquake data and using the station AG13 as reference (hereinafter real spectral ratios).

The numerical simulations were carried out starting from a simple model characterized by a homogenous basin infill above the substratum. The basin shape is based on results of the active source seismic tomography survey of Improta et alii (2008). We then varied the basin geometry and the physical parameters of the propagation medium, and the source depth to attempt to refine the results. The final model of the basin, for which the source depth was set at 1500 m,

is shown in Figure 14, and the physical parameters of the three different bodies forming the model are reported in Table 2.

Body I represents the limestone substratum. The V_S value is derived from the tomographic V_P as large as 4800 m/sand assuming a V_P/V_S ratio of 2.0. Such a relatively large value is in agreement with results of a high-resolution 3D passive seismic tomography (Improta et alii, 2017) reporting V_P/V_S values above 2 for the fractured, water-bearing Mesozoic platform limestones of the VAB.

The basin interior is structured into two bodies: body II mimics the thick sequence of cemented clastic sediments (Middle-Late Pleistocene alluvial fans and slope breccias deposits), body III the finer and softer sediments mainly consisting of fluvio-lacustrine and alluvial deposits (Upper Pleistocene – Holocene) developed along the central-western sector of the basin, as well as in the near-surface (Figure 3).

Again, the V_S values are derived from the high-resolution active source tomography and assuming reasonable V_P/V_S ratios for the stiff cemented coarse clastic deposits (V_P/V_S = 2.2) and for the softer/finer fluvio-lacustrine and alluvial recent deposits (V_P/V_S around 3). Density values are from Dell'Aversana (2003).

The comparison between the simulated spectral ratios obtained from the final model (Figure 14 and Table 2) and the real spectral ratios is reported in Figure 16. To represent the curves obtained from earthquake data, we report both the horizontal components of the motion taken individually and the geometric mean of the two. Figure 16 shows a quite satisfactory agreement in terms of the fundamental frequency f_0 for all six stations in the basin. The match in terms of amplification factors is good for all the sites, but BNF and ITS. The worst case is BNF, due to the overestimation of the amplification factors which is evident not only near the fundamental frequency but in the whole frequency range affected by amplification phenomena. A possible

cause of the strong mismatch could be a lower impedance contrast of the real structure compared to the input model between the low velocity surface deposit and the underlying cemented fan, or the high sensitivity of the shape of the theoretical transfer function to variations in lateral velocity in proximity of seismic stations.

From Figure 15, we note that this simple 2D numerical simulation clearly illustrates surface waves generated at the basin edges and travelling inside the basin. The surface waves, summed to early S-wave reverberations, are responsible for a significant amplification and increase in duration of ground motion for sites in the central part of the basin. This result is consistent with the observed real data and strongly suggests the presence of 2-D propagation effects.

5. Discussion and conclusions

In this study, for the first time, earthquake data recorded along a transect in the central sector of the VAB are used to investigate site effects. Our survey provides valuable information on the seismic response.

We found evident phenomena of amplification in a wide range of frequencies (0.5 - 5 Hz) with fundamental frequency between 0.7 and 1 Hz and significant amplification factors. The value of the fundamental frequency f_0 varies by moving along the investigated transect, in accordance with the asymmetry of the structure of the basin. Of relevance, the position of the main amplification peak does not depend on the total thickness of the Quaternary sediments (i. e., depth of the basin substratum).

The BNF station is located in correspondence of the deepest depocenter of the basin but its fundamental frequency is significantly higher than that of the stations in the central part. The internal structure of the VAB in the investigated sector plays a fundamental role on the variability of the seismic response, which agrees only in a first approximation with a one-

dimensional numerical model. The most significant amplification phenomena and the lowest fundamental frequencies are found in the western sector, where the basin is thinner, but the filling is made of low-velocity fluvial-lacustrine and alluvial material with greater impedance contrast with respect to the substratum. In the eastern sector, where the maximum depocenter of the basin is found, the filling is made of high-velocity cemented alluvial fan and slope breccias deposits, so the impedance contrast is lower (this explains the lower amplification factor and the shift of the fundamental resonance peak towards higher frequencies).

The effect of the presence of important lateral heterogeneities within the basin becomes evident while observing the response of the two stations located near the edges BNF and LMB (Figure 7); in the first case the amplification factors are lower (about 2), for LMB the peak moves to a higher frequency than that of BNF and the amplification factor is higher.

This difference is only partially reproduced by 2D simulations, thus indicating that despite the good control on the subsurface structure (in particular on the geometry), more complex 2D models and possibly 3D models are needed to reproduce the complexities found in the seismic response.

Our analysis of earthquake data supported by 2D simulations however highlights an important role of border effects, which cause the generation of surface wave trains that propagate from the edges through the entire basin. These packets of surface waves interfering with each other determine an increase in the amplitude of the motion and in its duration, mainly in correspondence with the sites in the central part of the basin (Figure 15).

The results of our study show a complex local seismic response that is strongly controlled by the internal structure of the basin. This suggests that in order to evaluate the local seismic response in other sectors of the VAB it is necessary to acquire new seismic data and take into account the complexity of the subsoil structure, which is determined by several elements,

among which the fundamentals are: i) the extension and thickness of fan bodies and slope breccias consisting of cemented coarse deposits that are present discontinuously mainly along the eastern edge of the basin; ii) the extension and thickness of fluvio-lacustrine deposits and recent alluvia of the Agri river that tend to thicken going towards the western edge of the basin (Zembo et alii, 2009); iii) the type and morphology of the pre-quaternary substrate.

In fact 2-D/3-D geophysical investigations show that the morphology of the substrate is very complex (Rizzo and Giampaolo, 2018), both in the longitudinal and transversal direction of the basin due to the presence of various structural lows and highs. In addition we expect a different seismic site response, with respect to the area investigated in this study, in the southernmost part of the basin where the substratum mainly consists of Cenozoic terrigenous deposits (sandstone, clay, shales) characterized by seismic velocities and densities lower than that of the Mesozoic limestones forming the substratum of the central-northern basin.

Our study evidences significant phenomena of amplification in duration and amplitude in a wide range of frequencies, with relevant amplification factors especially in the low frequency range (up to 7) related to the resonance of the entire basin and to the propagation of surface waves generated at the edges. Therefore it suggests that for an accurate assessment of the seismic hazard at the scale of the basin, it is necessary to take into account its extremely complex structure.

We found that the fundamental frequencies obtained with the HVSR technique are in excellent agreement with those derived from the SSR analysis of earthquake weak motion data. This suggests that the fundamental frequency f0 of the basin could be mapped in the whole VAB also using single station techniques. On the other hand, the evident underestimation of the amplification factors provided by the H/V spectral ratios of noise and earthquake data confirms

that earthquake recordings at a dense network are required to capture the basin site effects (Bard et alii, 1999; Di Giulio et alii, 2008).

Our experimental results can be useful for future studies on the seismic risk assessment of the residential buildings, civil infrastructure and industrial facilities of the Val d'Agri.

References

BARD, P.-Y., 1999, *Microtremor measurements: A tool for site effect estimation?*, in: Irikura, Kudo, Okada and Sasatani (eds.), Stateof-the-Art Paper, Second International Symposium on the Effects of Surface Geology on Seismic Motion, Yokohama, December, 1–3, 1998. Balkema, Vol. 3, pp. 1251–1279

BORCHERDT R. D. (1970). *Effects of local geology on ground motion near San Francisco Bay*. Bull. Seismol. Soc. Am. 60:29–61.

BORFECCHIA, F., G. DE CANIO, L. DE CECCO, A. GIOCOLI, S. GRAUSO, L. LA PORTA, S. MARTINI, M. POLLINO, I. ROSELLI, A. ZINI (2016). *Mapping the earthquake-induced landslide hazard around the main oil pipeline network of the Agri Valley (Basilicata, southern Italy) by means of two GIS-based modelling approaches.* Nat Hazards 81, 759–777 (2016). https://doi.org/10.1007/s11069-015-2104-0

BURRATO P. and VALENSISE G. (2008). *Rise and fall of a hypothesized seismic gap: source complexity in the 16 December 1857, Southern Italy earthquake (Mw 7.0)*. Bull. Seism. Soc. Am. 98 (1), 139-148. doi: 10.1785/0120070094.

CASERTA, A., 1998. *A time domain finite-difference technique for oblique incidence of antiplane waves in heterogeneous dissipative media.* Ann. Geophys., 41, 617– 631.

CASERTA, A., V. RUGGIERO, and P. LANUCARA (2002). *Numerical modelling of dynamical interaction between seismic radiation and near surface geological structures: A parallel approach.* Comput. Geosci., 28(9), 1069–1077.

CELLO, G., E. TONDI, L. MICARELLI, L. MATTIONI, 2003. *Active tectonics and earthquake sources in the epicentral area of the 1857 Basilicata earthquake (southern Italy)*. Journal of Geodynamics, Volume 36, Issues 1–2, pp 37-50, August–September 2003. https://doi.org/10.1016/S0264-3707(03)00037-1

DELL'AVERSANA, P., D. COLOMBO, M. BUIA, S. MORANDI, 2003. *Velocity/interface model building in a thrust belt by tomographic inversion of global offset seismic data*. Geophysical Prospecting, Volume 51, Issue 1, pp 23-35, January 2003. https://doi.org/10.1046/j.1365-2478.2003.00351.x

DI GIULIO, G., L. IMPROTA, G. CALDERONI, A. ROVELLI (2008). *A study of the seismic response of the city of Benevento (southern Italy) through a combined analysis of seismological and geological data*. Engineering Geology, 97, 146-170.

FIELD, E. H., K. A. JACOB (1995). *Comparison and test of various site-response estimation techniques, including three that are not reference-site dependent.* Bull. of Seism. Society of America 85, 1127-1143, August 1995

GRAVES, R. W. and WALD, D. J. (2004). *Observed and Simulated Ground Motions in the San Bernardino Basin Region for the Hector Mine, California, Earthquake.* Bulletin of the Seismological Society of America, Vol. 94, No. 1, pp. 131–146, February 2004

HASKELL, N. A. (1960). *Crustal reflection of plane SH waves*, J. Geoph. Res., 65, 4147 – 4150.

MUCCIARELLI M., 2005: *Progetto di monitoraggio geofisico e di amplificazione sismica di sito di aree vulnerabili del territorio regionale.* Convenzione tra Regione Basilicata e Università della Basilicata, www.crisbasilicata.it/microzonazione/home.html.

IMPROTA, L., S. OPERTO, C. PIROMALLO AND L. VALOROSO (2008). *High-resolution imaging of basin-bounding normal faults in the Southern Apennines seismic belt (Italy) by traveltime and frequency-domain full-waveform tomography*. 70th EAGE Conference and Exhibition - Workshops and Fieldtrips, Jun 2008, cp-41-00073. DOI: https://doi.org/10.3997/2214-4609.201405066

IMPROTA, L., L. FERRANTI, P. M. DE MARTINI, S. PISCITELLI, P. P. BRUNO, P. BURRATO, R. CIVICO, A. GIOCOLI, M. IORIO, G. D'ADDEZIO, L. MASCHIO, 2010. *Detecting young, slow-slipping active faults by geologic and multidisciplinary high-resolution geophysical investigations: A case study from the Apennine seismic belt, Italy*.

Journal of Geophysical Research, Volume 115, Issue B11, November 2010. https://doi.org/10.1029/2010JB000871

IMPROTA L., L. VALOROSO, D. PICCININI, C. CHIARABBA, 2015. *A detailed analysis of wastewater-induced seismicity in the Val d'Agri oil field (Italy)*. Geophysical Research Letters, Volume 42, Issue 8, pp 2682-2690, 2015. https://doi.org/10.1002/2015GL063369

IMPROTA., L., S. BAGH, P. DE GORI, L. VALOROSO, M. PASTORI, D. PICCININI, C. CHIARABBA, M. ANSELMI, M. BUTTINELLI, 2017. *Reservoir Structure and Wastewater-Induced Seismicity at the Val d'Agri Oilfield (Italy) Shown by Three-Dimensional Vp and Vp/Vs Local Earthquake Tomography*. JGR Solid Earth, Volume 122, Issue 11, pp 9050-9082, November 2017. https://doi.org/10.1002/2017JB014725.

LACHET, C., P.-Y. BARD (1994). *Numerical and theoretical investigations on the possibilities and limitations of the Nakamura's technique.* J. Physics of the Earth, 42-4, 377-397.

MALLET R., (1862). *Great Neapolitan earthquake of 1857. The first principles of observational seismology,* Londra.

MASCHIO, L., L. FERRANTI, P. BURRATO, 2005. *Active extension in Val d'Agri area, Southern Apennines, Italy: implications for the geometry of the seismogenic belt*. Geophysical Journal International, Volume 162, Issue 2, pp 591–609, August 2005. https://doi.org/10.1111/j.1365-246X.2005.02597.x

MASI, A., V. MANFREDI and G. NICODEMO, 2021. *Seismic rehabilitation of residential buildings: an action plan for the urban centres in Val d'Agri, Italy.* Bollettino di Geofisica Teorica ed Applicata, Vol. 62, n. 2, pp. 243-268; June 2021. DOI 10.4430/bgta0333

MORANDI, S. and E. CERAGIOLI, 2002. *Integrated interpretation of seismic and resistivity images across the Val d'Agri graben (Italy)*. ANNALS OF GEOPHYSICS, VOL. 45, N. 2, April 2002. https://doi.org/10.4401/ag-3510

NAKAMURA, Y. (1989). *A method for dynamic characteristics estimation of subsurface using microtremor on the ground surface*. Quarterly Reports of Railway Technical Research Institute (RTRI), 30, 25-33.

RIZZO, E. & GIAMPAOLO V. (2019). *New deep electrical resistivity tomography in the High Agri Valley basin (Basilicata, Southern Italy),* Geomatics, Natural Hazards and Risk, 10:1, 197-218, DOI: 10.1080/19475705.2018.1520150

RUGGIERO, V., P. LANUCARA, M. P. BUSICO, A. CASERTA, AND B. FIRMANI (2004). *Numerical modelling of the ground motion: A parallel approach for finite element methods*. In Proceedings of the 7th Conference on Applied and Industrial Mathematics in Italy, pp. 487–495, World Scientific, Venice, Italy.

SANTONI D., GIUFFRIDA, C., RUGGIERO, V., CASERTA, A. & LANUCARA, P., 2004. *Web user-friendly interface to produce input data for numerical simulations of seismic wave propagation.* EGS-AGU-EUG Joint Assembly, Nice, France (poster).

SITE EFFECTS ASSESSMENT USING AMBIENT EXCITATIONS (SESAME) EUROPEAN PROJECT (2005) Deliverable D23.12 — *Guidelines for the implementation of the H/V spectral ratio technique on ambient vibrations measurements, processing and interpretation*. Bulletin of Earthquake Engineering - March 2008.

STABILE, T. A., A. GIOCOLI, A. PERRONE, S. PISCITELLI, V. LAPENNA, 2014. *Fluid injection induced seismicity reveals a NE dipping fault in the southeastern sector of the High Agri Valley (southern Italy)*. Geophysical Research Letters, Volume 41, Issue 16, pp. 5847–5854, 2014. https://doi.org/10.1002/2014GL060948

STABILE, T. A., A. GIOCOLI, A. PERRONE, S. PISCITELLI, L. TELESCA and V. LAPENNA (2015). *Relationship between seismicity and water level of the Pertusillo reservoir (southern Italy)*. Bollettino di Geofisica Teorica ed Applicata Vol. 56, n. 4, pp. 505-517; December 2015. DOI 10.4430/bgta0161

VALOROSO, L., L. IMPROTA, L. CHIARALUCE, R. DI STEFANO, L. FERRANTI, A. GOVONI, C. CHIARABBA, 2009. *Active faults and induced seismicity in the Val d'Agri area (Southern Apennines, Italy)*. Geophysical Journal International, Volume 178, Issue 1, pp 488–502, July 2009. https://doi.org/10.1111/j.1365-246X.2009.04166.x

ZEMBO, I., VIGNOLA, P., ANDÒ, S. ET AL., 2009. *Tephrochronological study in the quaternary Val d'Agri intermontane basin (Southern Apennines, Italy).* Int. J. Earth Sci. (Geol. Rundsch) 100, 173–187 (2011). https://doi.org/10.1007/s00531-009-0501-x

Figure captions

Figure 1. Geologic map of the Val d'Agri basin and surrounding regions (modified after Lazzari and Lentini [1991]). 1 – Quaternary continental deposits; 2 – Flysch sediments of satellite basins (Middle Miocene-Pliocene); 3 – Pelagic and slope successions (Cretaceous-Lower Miocene); 4 – Mesozoic rocks of the Lagonegro Basin; 5 – Western Carbonate Platform (Mesozoic); 6 - Apulia Carbonate Platform IAP (Mesozoic – Miocene); 7 – main reverse faults and overthrusts; 8 – antiform axis; 9 – normal faults; EAFS – Eastern Agri Fault System; MMFS – Mts. Maddalena Fault System. EAFS dips toward SW [Cello et alii, 2003], MMFS dips toward NE [Maschio et alii, 2005]. The dashed box indicates the sector of the basin investigated in this study where we installed the temporary network (shown in map in Figure 2). The thick black line is the trace of the seismic profile shown in Figure 3. The inset map on the right shows the main basins and ridges in the region and the Pertusillo lake.

Figure 2. Geologic map of the central sector of Val d'Agri basin investigated in this study (modified after Lazzari and Lentini [1991]). The seismic stations of the 2006-2009 temporary network are depicted by blue and red triangles (stations deployed on limestone bedrock and on basin sediments, respectively). The thick black line is the trace of the seismic profile shown in Figure 3. The central sector of the basin is outlined in Figure 1.

Figure 3. (upper panel) P-wave velocity model of the central sector of the basin (modified after Improta et alii, 2008). The model strikes SW-NE and was obtained by a refraction tomography survey of the multifold wide-aperture seismic profile that crosses the central part of the basin (Dell'Aversana, 2003). The red and blue triangles are stations of the 2006-2009 seismic experiment (limestone bedrock and basin stations, respectively). The basin substratum composed of Mesozoic fractured limestone of the Western Carbonate Platform (see Figures 1 and 2) corresponds to the high-V_P regions (V_P > 4500 m/s). The basin infill attains velocities in the 500-2500 m/s range. (lower panel) Schematic model of the basin structure with outlined the two internal zones: (i) the eastern one mainly formed by Middle-Upper Pleistocene cemented coarse clastic sediments (slope breccias and alluvial fans; dark gray) and (ii) the central-western one mainly composed of Upper Pleistocene - Holocene alluvia and fluvio-lacustrine deposits (light gray).

Figure 4 –Epicenters of the earthquakes used in the analysis; the blue triangle indicates the position of the VAB.

Figure 5 - Average HVSR on earthquakes and noise for stations AG13 and AG44

Figure 6 - Waveforms of the horizontal components of a regional event used in the analysis (lat 39.28, lon 16.96, 2007-03-26 13:55:26, Mw 3.8)

Figure 7 - Average SSRs with respect to the reference site AG13 for all the stations in the basin

Figure 8a - average HVSR on earthquakes and noise for stations AAP, AAS, CFS

Figure 8b - average HVSR on earthquakes and noise for stations ITS, BNF, LMB

Figure 9 - Amplitude of theoretical transfer function for station AAS resulting from 1D modeling

Figure 10 – Waveforms of the horizontal components for a Campanian-Lucanian Apennine event showing a clear increase in ground motion duration for basin sites.

Figure 11 – Campanian-Lucanian Apennine event: spectral ratios of the stations in the basin with respect to AG13, for horizontal components of motion

Figure 12 - Campanian-Lucanian Apennine event: spectrograms of stations AAS and AG13

Figure 13 - Campanian-Lucanian Apennine event: seismograms of stations AAS e AG13 (left panel), particle motion of AAS (right panel) made using the time window delimited by the two vertical lines

Figure 14–Geometry of the final model with the three bodies denoted by roman numbers (see the text). The dashed line represents the position of the forcing term. The blue circles are the seismic stations projected on the model.

Figure 15 - Plot of synthetic seismograms obtained from the final 2D simulation. One site out of every 5 is displayed.

Figure 16 - Comparison between spectral ratios obtained from the final numerical simulation and those obtained from the application of the SSR technique to earthquake recordings at seismic stations

Tables

station	V_S (m/s)	thickness (m)
AAP	1210	480

AAS	1273	465
CFS	1262	340
ITS	1050	336

Table 1 - S-wave velocity and thicknesses for the most superficial layer used in 1-D models

body	V_S (m/s)	density (g/cm^3)	Q factor
I	2400	2.6	15
II	1000	2.2	15
III	500	1.8	15

Table 2 - Physical properties of the bodies used in the final model

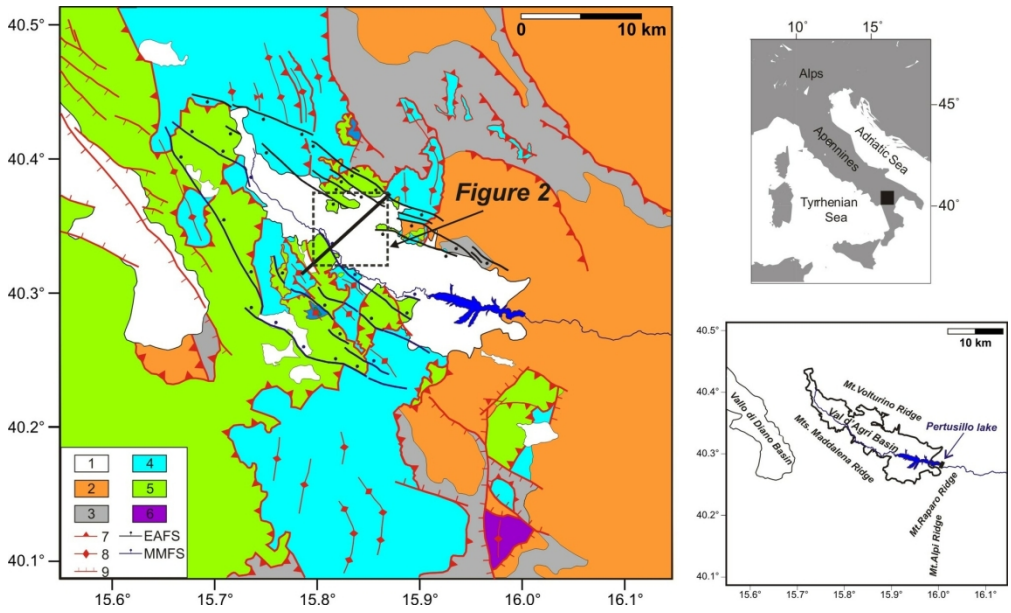

Figure 1. Geologic map of the Val d'Agri basin and surrounding regions (modified after Lazzari and Lentini [1991]). 1 – Quaternary continental deposits; 2 – Flysch sediments of satellite basins (Middle Miocene-Pliocene); 3 – Pelagic and slope successions (Cretaceous-Lower Miocene); 4 – Mesozoic rocks of the Lagonegro Basin; 5 – Western Carbonate Platform (Mesozoic); 6 - Apulia Carbonate Platform IAP (Mesozoic – Miocene); 7 – main reverse faults and overthrusts; 8 – antiform axis; 9 – normal faults; EAFS – Eastern Agri Fault System; MMFS – Mts. Maddalena Fault System. EAFS dips toward SW [Cello et alii, 2003], MMFS dips toward NE [Maschio et alii, 2005]. The dashed box indicates the sector of the basin investigated in this study where we installed the temporary network (shown in map in Figure 2). The thick black line is the trace of the seismic profile shown in Figure 3. The inset map on the right shows the main basins and ridges in the region and the Pertusillo lake.

171x102mm (300 x 300 DPI)

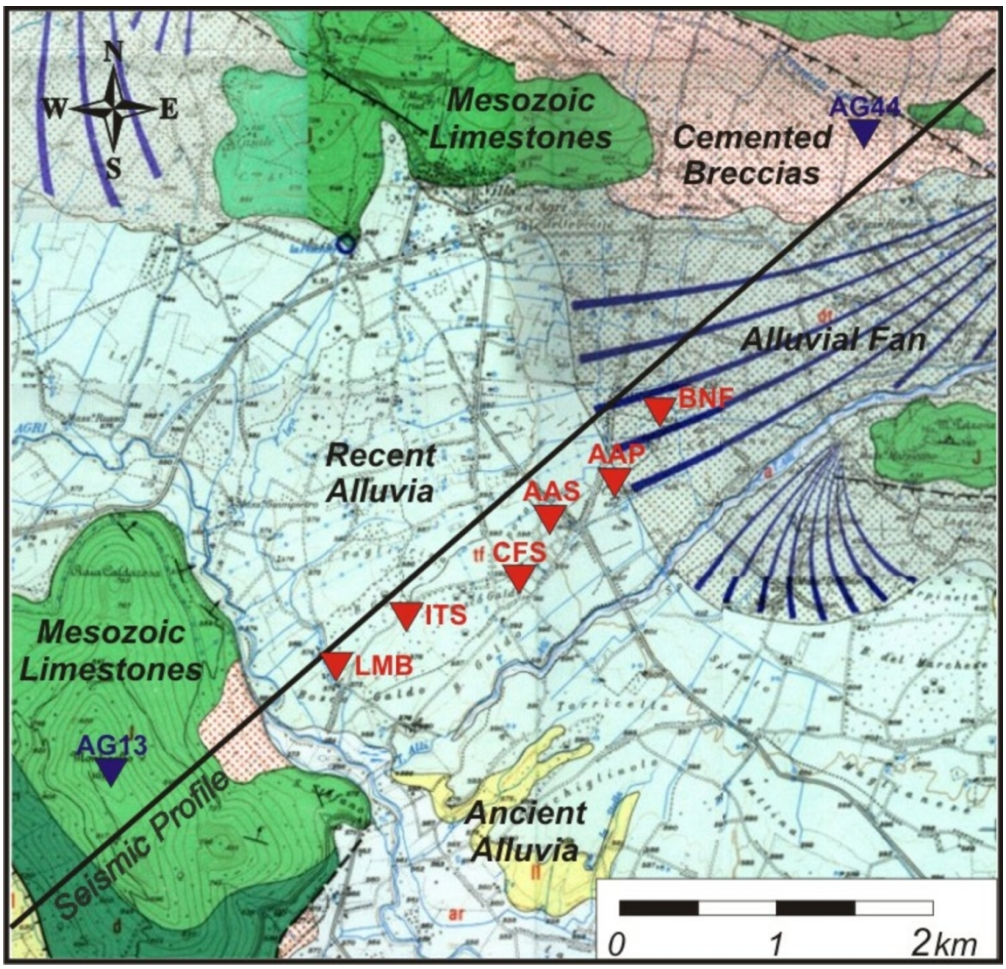

Figure 2. Geologic map of the central sector of Val d'Agri basin investigated in this study (modified after Lazzari and Lentini [1991]). The seismic stations of the 2006-2009 temporary network are depicted by blue and red triangles (stations deployed on limestone bedrock and on basin sediments, respectively). The thick black line is the trace of the seismic profile shown in Figure 3. The central sector of the basin is outlined in Figure 1.

127x122mm (300 x 300 DPI)

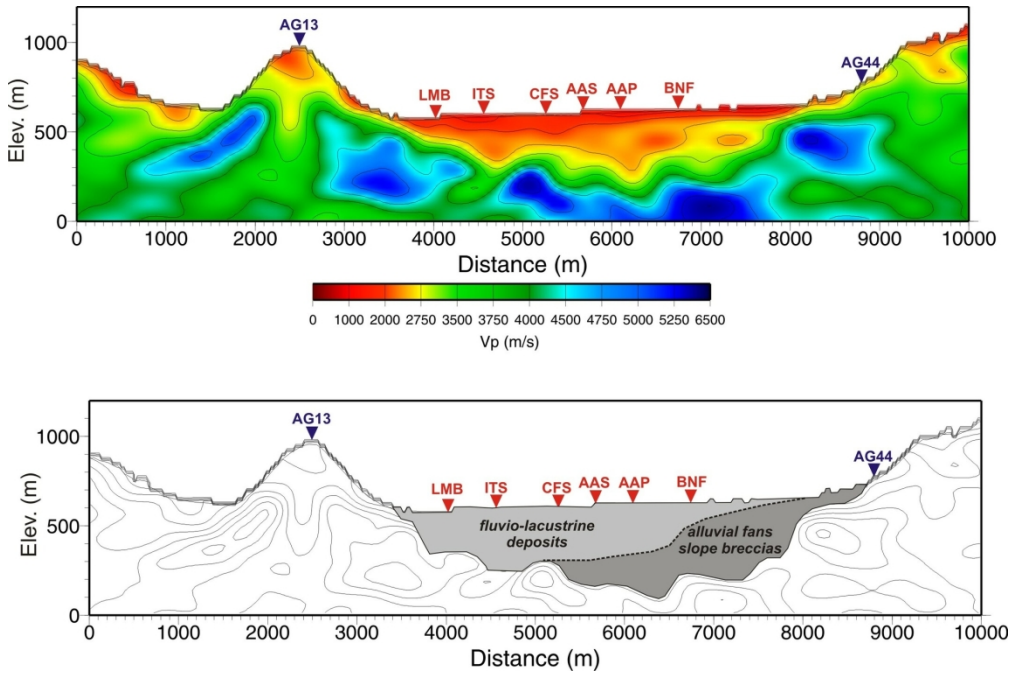

Figure 3. (upper panel) P-wave velocity model of the central sector of the basin (modified after Improta et alii, 2008). The model strikes SW-NE and was obtained by a refraction tomography survey of the multifold wide-aperture seismic profile that crosses the central part of the basin (Dell'Aversana, 2003). The red and blue triangles are stations of the 2006-2009 seismic experiment (limestone bedrock and basin stations, respectively). The basin substratum composed of Mesozoic fractured limestone of the Western Carbonate Platform (see Figures 1 and 2) corresponds to the high-VP regions (VP > 4500 m/s). The basin infill attains velocities in the 500-2500 m/s range. (lower panel) Schematic model of the basin structure with outlined the two internal zones: (i) the eastern one mainly formed by Middle-Upper Pleistocene cemented coarse clastic sediments (slope breccias and alluvial fans; dark gray) and (ii) the central-western one mainly composed of Upper Pleistocene - Holocene alluvia and fluvio-lacustrine deposits (light gray).

181x120mm (300 x 300 DPI)

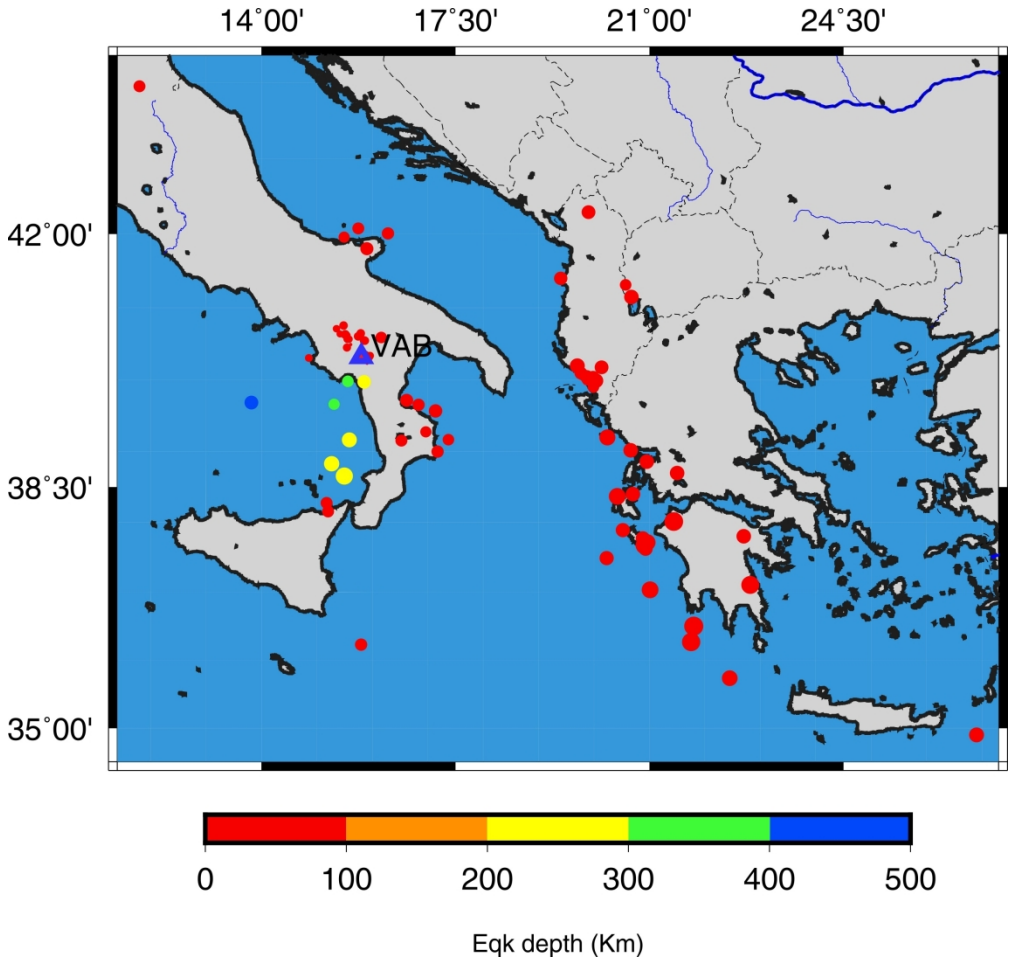

Figure 4 –Epicenters of the earthquakes used in the analysis; the blue triangle indicates the position of the VAB.

405x384mm (168 x 168 DPI)

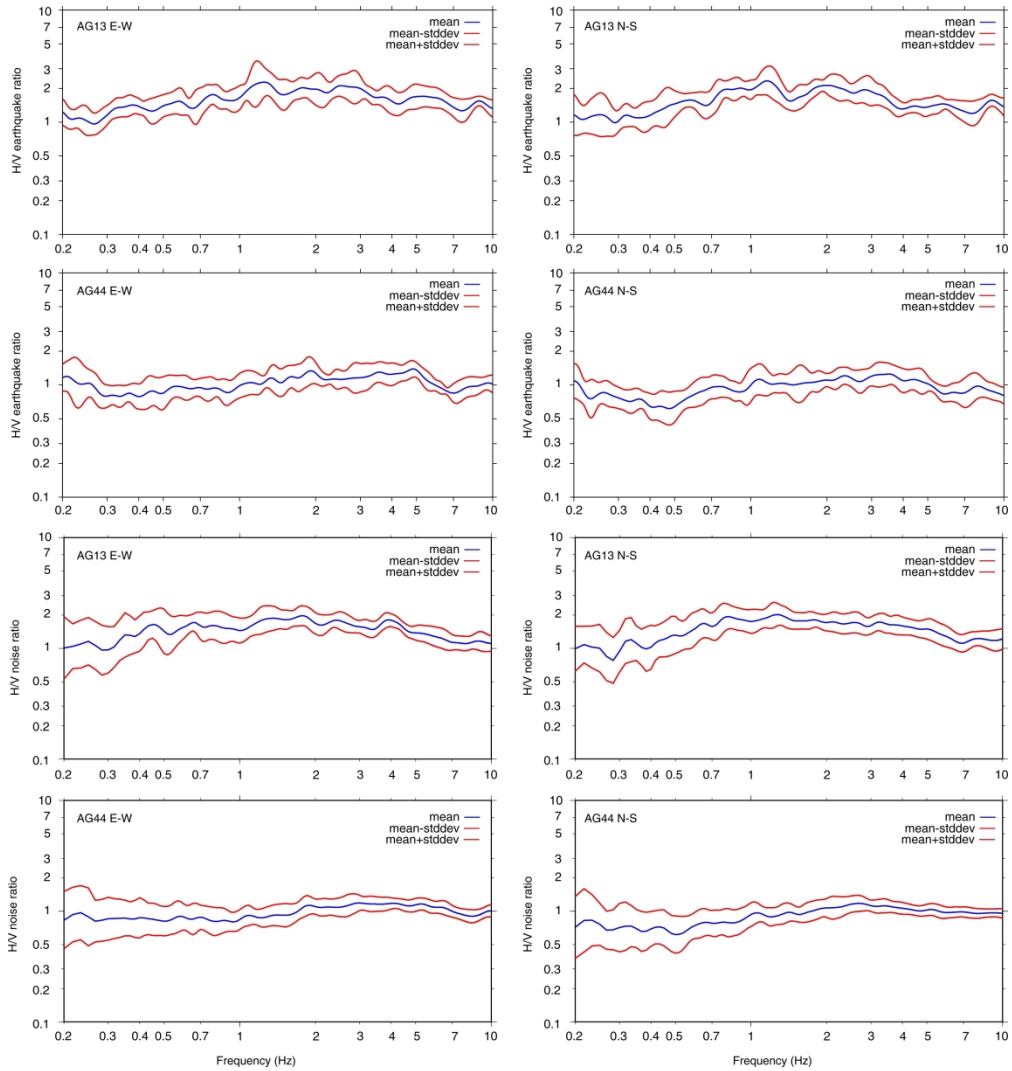

Figure 5 - Average HVSR on earthquakes and noise for stations AG13 and AG44

472x501mm (168 x 168 DPI)

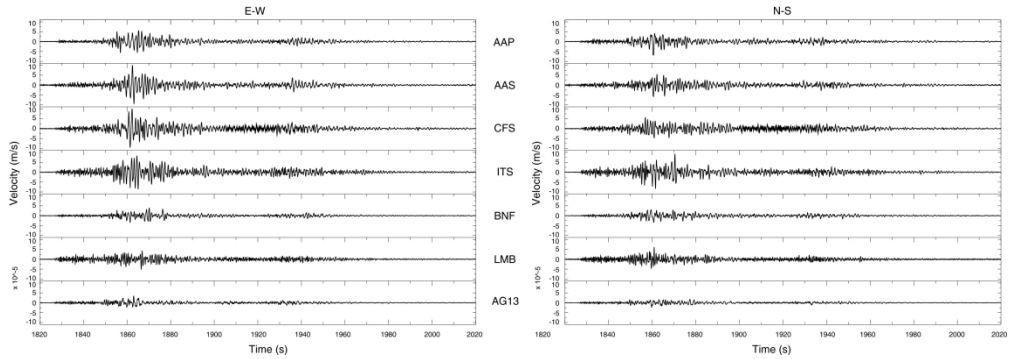

Figure 6 - Waveforms of the horizontal components of a regional event used in the analysis (lat 39.28, lon 16.96, 2007-03-26 13:55:26, Mw 3.8)

566x197mm (168 x 168 DPI)

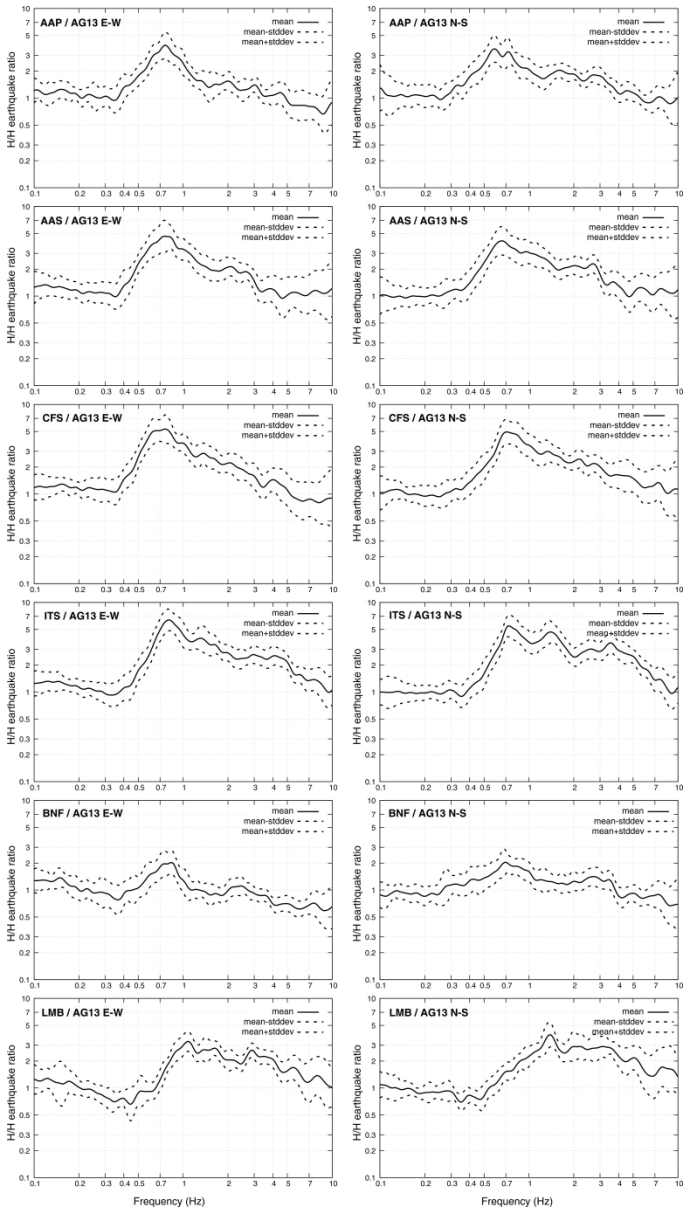

Figure 7 - Average SSRs with respect to the reference site AG13 for all the stations in the basin

472x837mm (168 x 168 DPI)

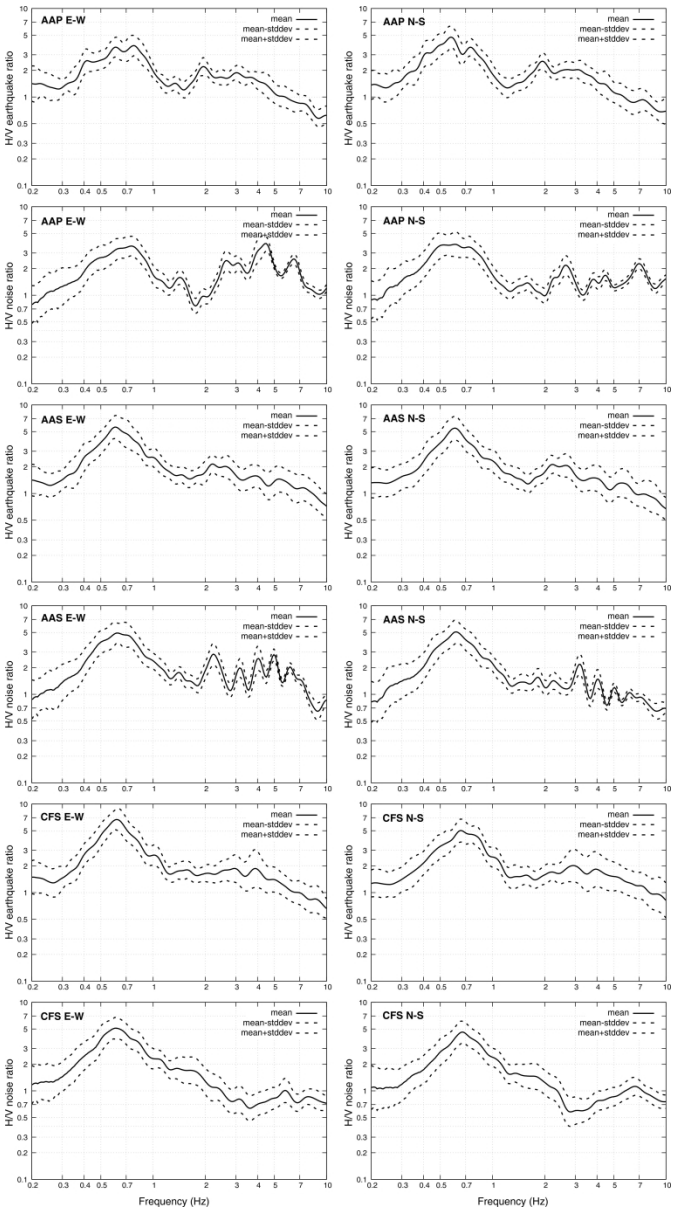

Figure 8a - average HVSR on earthquakes and noise for stations AAP, AAS, CFS

472x850mm (168 x 168 DPI)

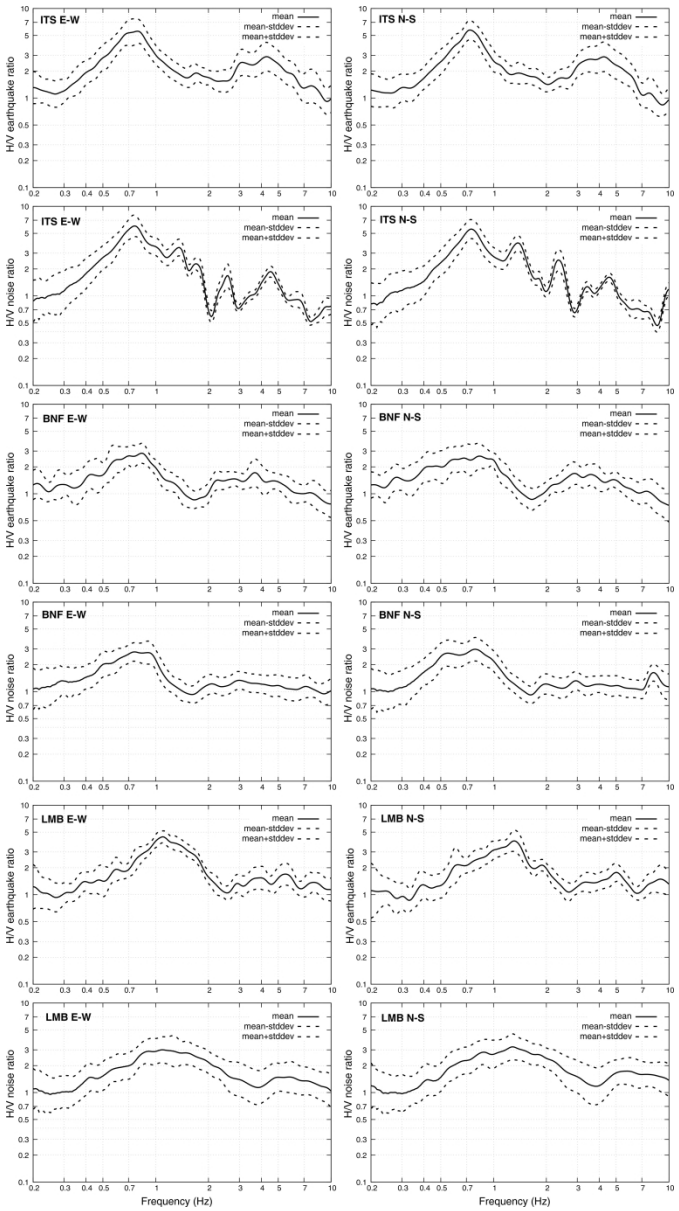

Figure 8b - average HVSR on earthquakes and noise for stations ITS, BNF, LMB

472x848mm (168 x 168 DPI)

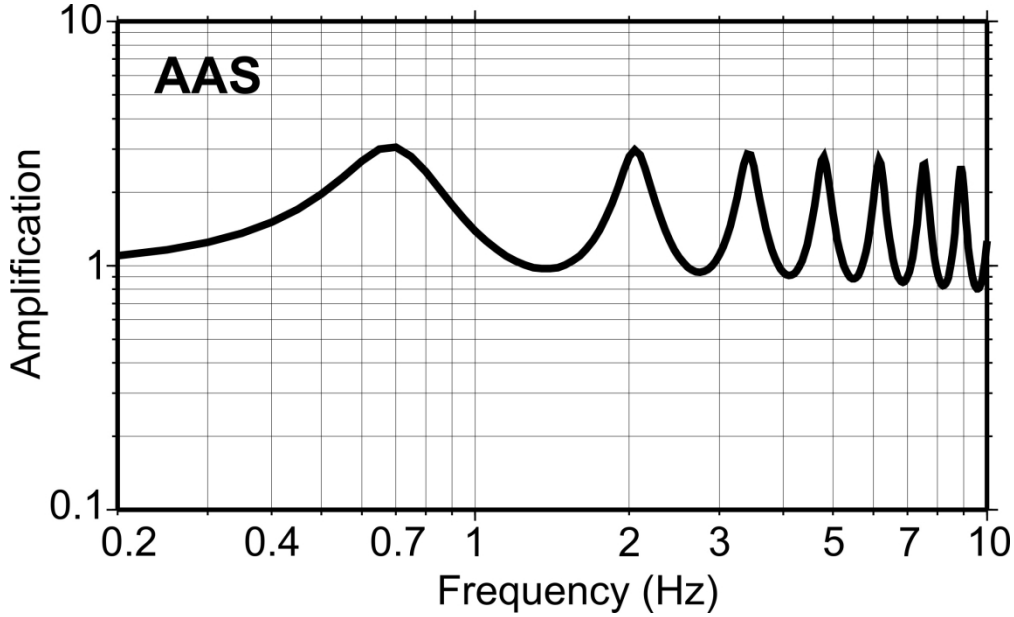

Figure 9 - Amplitude of theoretical transfer function for station AAS resulting from 1D modeling

377x230mm (168 x 168 DPI)

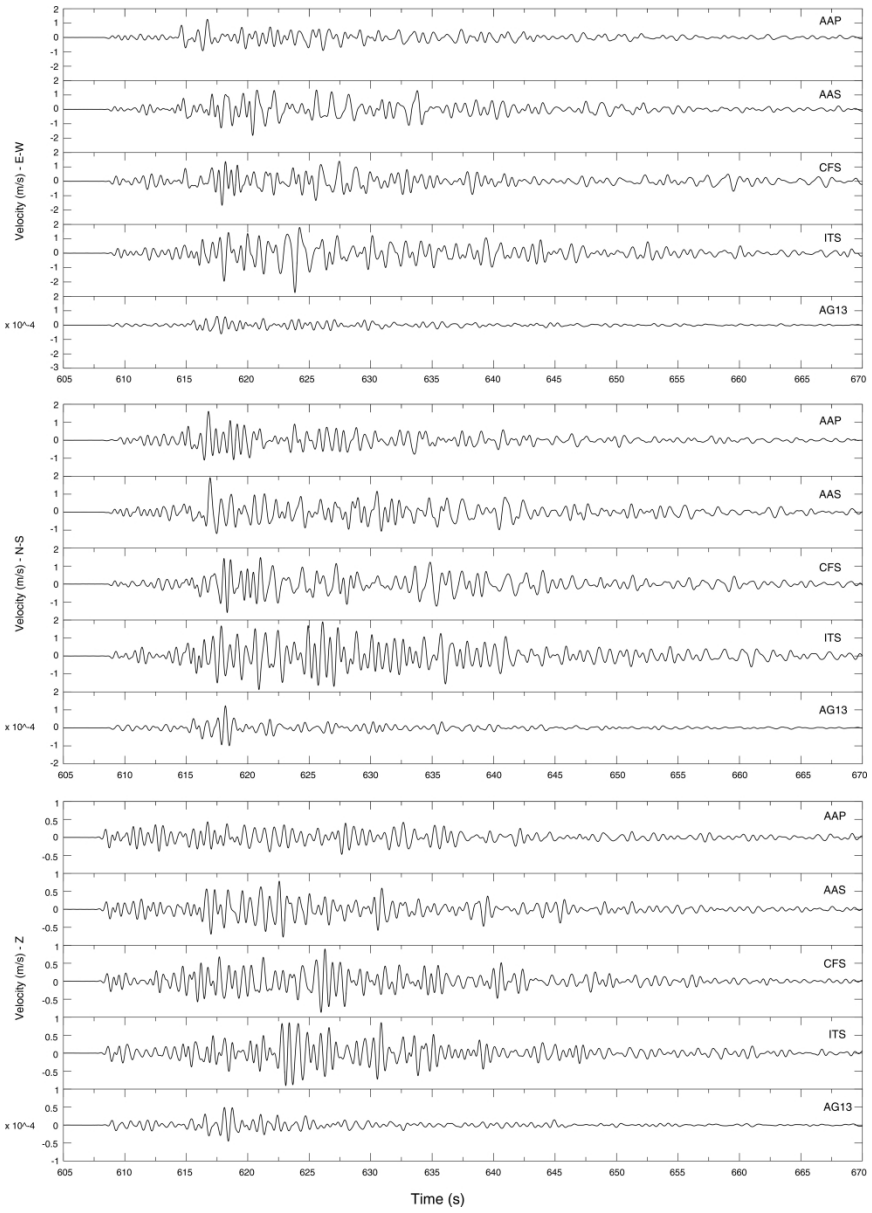

Figure 10 – Waveforms of the horizontal components for a Campanian-Lucanian Apennine event showing a clear increase in ground motion duration for basin sites.

587x816mm (168 x 168 DPI)

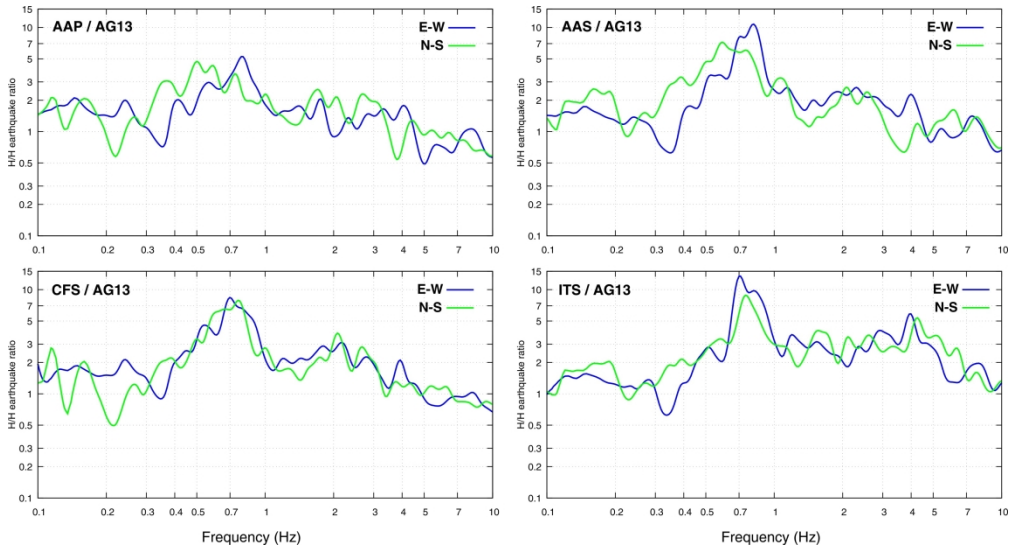

Figure 11 – Campanian-Lucanian Apennine event: spectral ratios of the stations in the basin with respect to AG13, for horizontal components of motion

472x254mm (168 x 168 DPI)

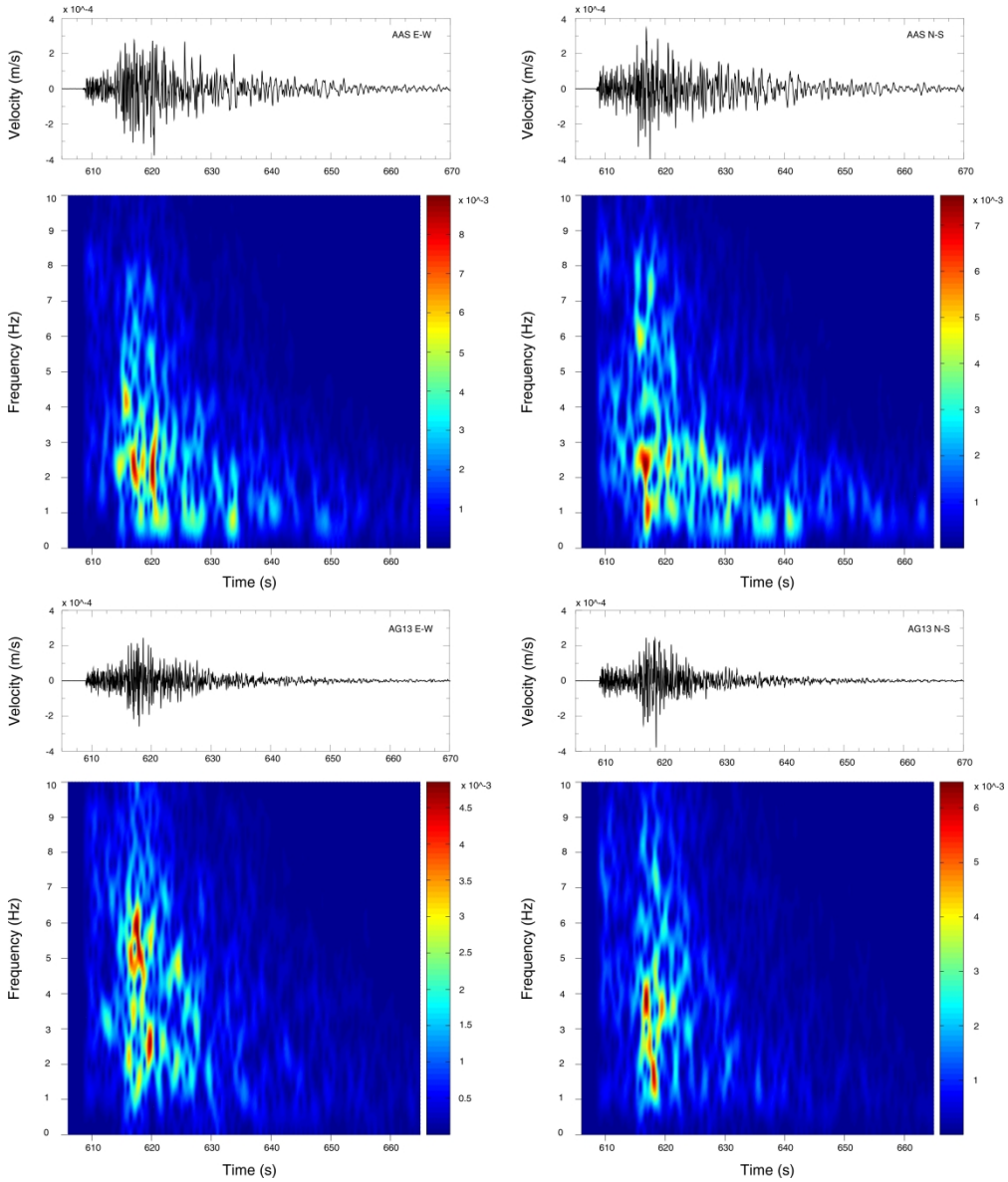

Figure 12 - Campanian-Lucanian Apennine event: spectrograms of stations AAS and AG13

614x721mm (168 x 168 DPI)

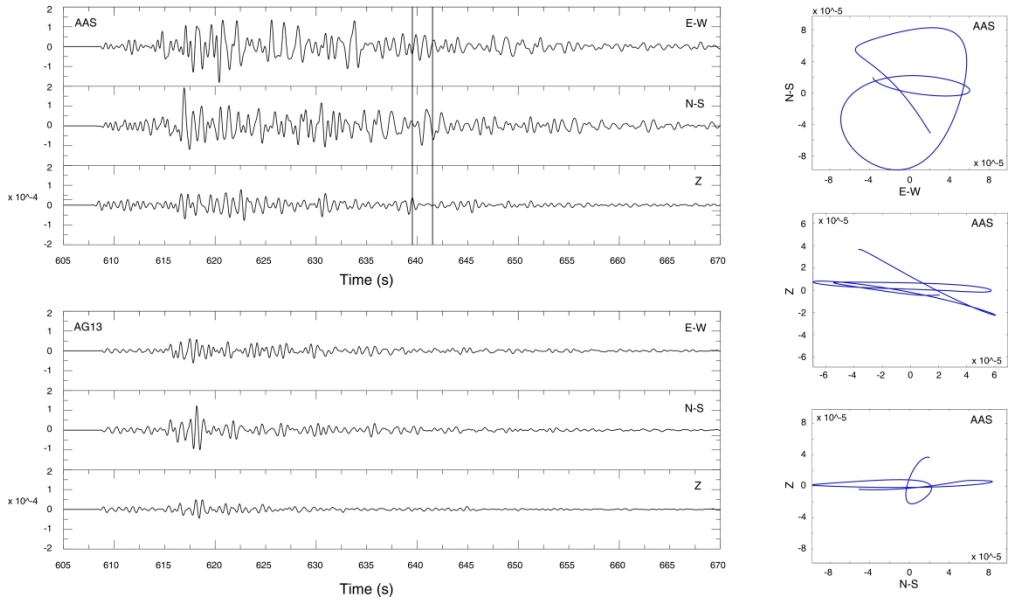

Figure 13 - Campanian-Lucanian Apennine event: seismograms of stations AAS e AG13 (left panel), particle motion of AAS (right panel) made using the time window delimited by the two vertical lines

614x362mm (168 x 168 DPI)

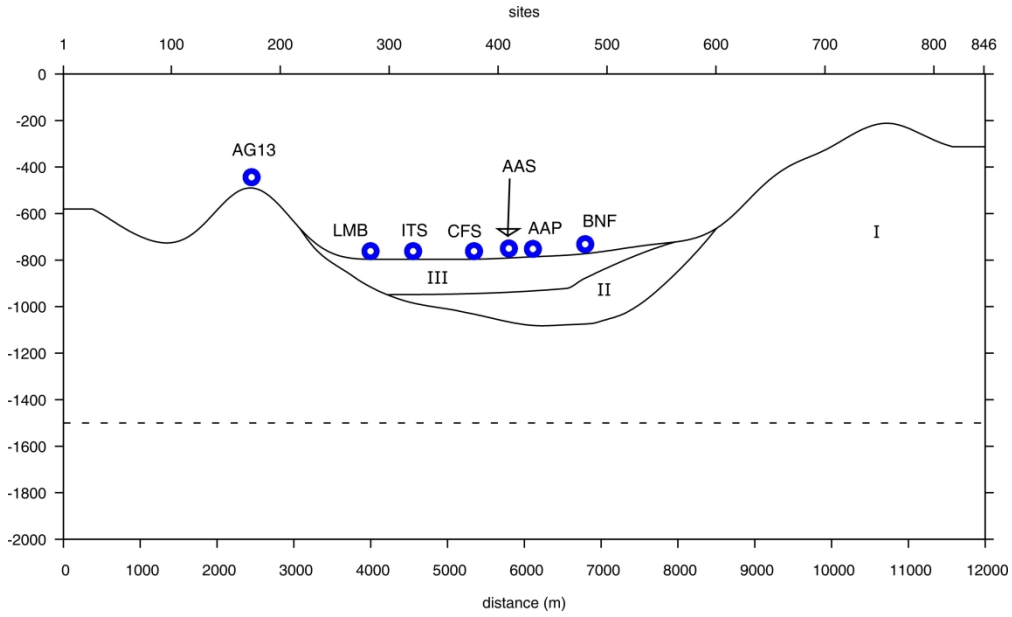

Figure 14–Geometry of the final model with the three bodies denoted by roman numbers (see the text). The dashed line represents the position of the forcing term. The blue circles are the seismic stations projected on the model.

472x286mm (168 x 168 DPI)

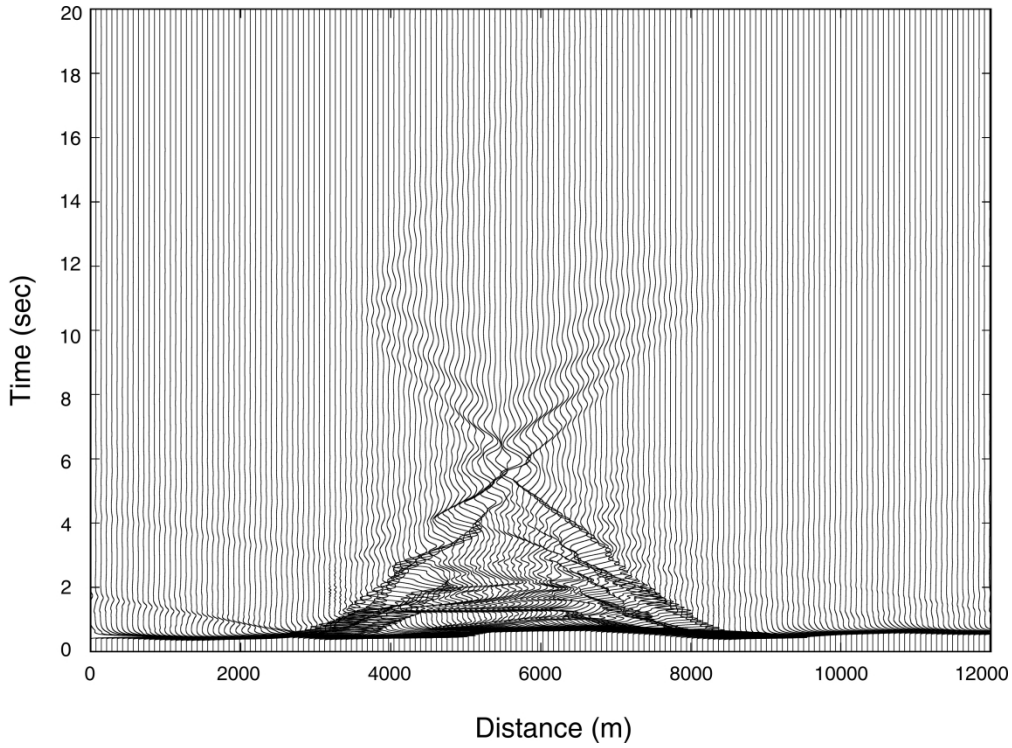

Figure 15 - Plot of synthetic seismograms obtained from the final 2D simulation. One site out of every 5 is displayed.

519x382mm (168 x 168 DPI)

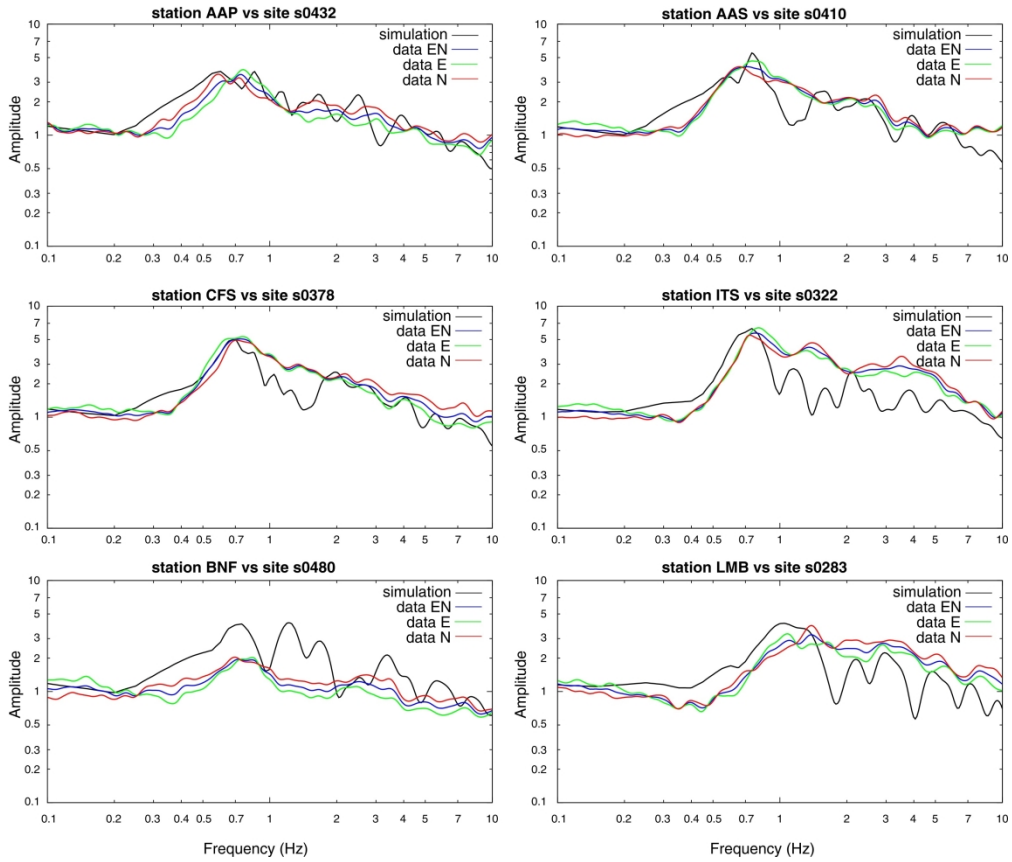

Figure 16 - Comparison between spectral ratios obtained from the final numerical simulation and those obtained from the application of the SSR technique to earthquake recordings at seismic stations

472x401mm (168 x 168 DPI)